# Effect of dispersed phase viscosity on maximum droplet generation frequency in microchannel emulsification using asymmetric straight-through channels

Goran T. Vladisavljević[a,b*], Isao Kobayashi[c*], Mitsutoshi Nakajima[c,d]

[a]*Chemical Engineering Department, Loughborough University, Loughborough, Leicestershire LE11 3TU UK.*

[b]*Vinča Insitute of Nuclear Sciences, Laboratory of chemical dynamics, P.O.Box 522, 11001 Belgrade, Serbia.*

[c]*National Food Research Institute, National Agriculture and Food Research Organization, Kannondai 2-1-12, Tsukuba, Ibaraki, Japan 305-8642.*

[d]*Graduate School of Life and Environmental Sciences, University of Tsukuba, 1-1-1, Tennoudai, Tsukuba, Ibaraki, Japan 305-8572*.

[*]Corresponding authors. E-mails: G.Vladisavljevic@lboro.ac.uk (G.T. Vladisavljević), isaok@affrc.go.jp (I. Kobayashi).



Vladisavljević, G.T., Kobayashi, I. and Nakajima, M (2011) Microfluid Nanofluid 10: 1999–1209

**Abstract**

Uniformly sized droplets of soybean oil, MCT (medium-chain fatty acid triglyceride) oil and n-tetradecane with a Sauter mean diameter of $d_{3,2}$ = 26–35 μm and a distribution span of 0.21–0.25 have been produced at high throughputs using a 24 × 24 mm silicon microchannel plate consisting of 23,348 asymmetric channels fabricated by photolithography and deep reactive ion etching. Each channel consisted of a 10-μm diameter straight-through micro-hole with a length of 70 μm and a 50 × 10 μm micro-slot with a depth of 30 μm at the outlet of each channel. The maximum dispersed phase flux for monodisperse emulsion generation increased with decreasing dispersed phase viscosity and ranged from over 120 L $m^{-2}$ $h^{-1}$ for soybean oil to 2700 L $m^{-2}$ $h^{-1}$ for n-tetradecane. The droplet generation frequency showed significant channel to channel variations and increased with decreasing viscosity of the dispersed phase. For n-tetradecane, the maximum mean droplet generation frequency was 250 Hz per single active channel, corresponding to the overall throughput in the device of 3.2 million droplets per second. The proportion of active channels at high throughputs approached 100% for soybean oil and MCT oil and 50% for n-tetradecane. The agreement between the experimental and CFD (Computational Fluid Dynamics) results was excellent for soybean oil and the poorest for n-tetradecane.

**Keywords** Microchannel emulsification · Membrane emulsification · Single crystal silicon microchannel array · Droplet generation frequency · Monodisperse droplets



Vladisavljević, G.T., Kobayashi, I. and Nakajima, M (2011) Microfluid Nanofluid 10: 1999–1209

**List of Symbols**

| | |
|---|---|
| $A_m$ | Active cross sectional area of microchannel plate ($m^2$) |
| $Ca$ | Capillary number (–) |
| $d$ | Droplet diameter (m) |
| $d_{10}$, $d_{50}$, $d_{90}$ | Droplet diameters corresponding to 10, 50, and 90% cumulative undersize mass (m) |
| $d_{3,2}$ | Sauter mean diameter of droplets (m) |
| $d_{ch}$ | Diameter of microchannel (m) |
| $k$ | fraction of active microchannels (–) |
| $h$ | Height of gap between microchannel plate and cover slip (m) |
| $N_0$ | Total number of microchannels in plate (–) |
| $Q$ | Volume flow rate ($m^3\ s^{-1}$) |
| $U$ | Velocity of disperse phase in microchannel ($m\ s^{-1}$) |
| $\bar{U}$ | mean velocity of disperse phase in active microchannels ($m\ s^{-1}$) |
| $W$ | Width of gap between MC plate and cover slip (m) |
| $We$ | Weber number (–) |
| $\gamma$ | Interfacial tension ($N\ m^{-1}$) |
| $\eta$ | Viscosity (Pa s) |
| $\rho$ | Density ($kg\ m^{-3}$) |
| $\tau$ | Shear stress (Pa) |

Subscripts

c refers to continuous phase



Vladisavljević, G.T., Kobayashi, I. and Nakajima, M (2011) Microfluid Nanofluid 10: 1999–1209

cr refers to critical conditions

d refers to disperse phase

## 1 Introduction

Over the past two decades, several microengineering techniques for drop-by-drop generation of size-controlled droplets have been developed. Membrane emulsification (ME) involves passing a pure dispersed phase through a microporous membrane into the continuous phase (direct ME) (Nakashima et al. 2000; Williams et al. 1998) or controlled breakup of pre-formed large droplets in the membrane pores (premix ME) (Vladisavljević et al. 2006). Various membrane configurations have been investigated for direct ME including cross-flow systems (Vladisavljević and Schubert, 2003a), rotating stainless steel tube with laser drilled pores (Vladisavljević and Williams, 2006), vibrating microsieve membrane (Holdich et al. 2010) and stirred cell with flat-disc membrane (Egidi et al. 2008). ME enables production of emulsions over a wide range of mean droplet sizes from about 0.3 μm to several hundred μm with a width of the particle size distribution typically in the range of 0.3–0.6 as measured by relative span factor (Table A1) or above 10% in terms of coefficient of variation (CV). The relative span factor is the relative width of a particle size distribution defined in Table A1.

Microfluidic droplet generators such as flow focusing devices (Anna et al. 2003; Xu and Nakajima 2004) and Ψ, Y or T junctions (Nisisako et al. 2006; Steegmans et al. 2009; Thorsen et al. 2001) can generate monodisperse droplets with a minimum size of around 10 μm and a CV of less than 3 %. These devices employ cross-, co-current- or counter-current flow of two immiscible liquids in microchannels (MCs) to form oil-in-water (O/W) or water-



Vladisavljević, G.T., Kobayashi, I. and Nakajima, M (2011) Microfluid Nanofluid 10: 1999–1209

in-oil (W/O) emulsion droplets (Thorsen et al. 2001; Nisisako et al. 2006; Utada et al. 2007). Alternatively, uniform droplets can be formed by passive breakup of large droplet plugs in microfluidic T-junctions or obstacles (Link et al. 2004). Core/shell droplets and higher-order multiple emulsion droplets can be generated by combining co- and counter-current flow (Utada et al. 2005) or using sequential droplet-formation units (DFUs) with alternating wettability (Abate and Weitz, 2009). Although droplet generation frequency in flow focusing devices can be up to 1,000 Hz for O/W emulsions and as high as 12,000 Hz for W/O emulsions (Yobas et al. 2006), flow rate of dispersed phase is usually very low, due to limited number of DFUs per chip. Nisisako and Torii (2006) developed a glass microfluidic chip with 256 DFUs (radially arranged Ψ- or cross- junctions) to produce droplets of photopolymerizable acrylate monomer at a throughput of 320 mL $h^{-1}$, but the particle diameter was around 100 μm. EDGE (Edge-based Droplet Generation) devices developed by van Dijke et al. (2009a) enable simultaneous generation of many droplets from a single rectangular microfluidic plateau. EDGE system was scaled up by incorporating 196 plateaus (DFUs) in a single chip by van Dijke et al. (2009b).

MC array devices can allow integration of hundreds of thousands of DFUs on a single chip (Kobayashi et al. 2005a) and the diameter of generated droplets can range from 1 μm (Kobayashi et al. 2007) to several mm (Kobayashi et al. 2008b). MC arrays can be fabricated parallel to the MC plate surface as open microgrooves (Kawakatsu et al. 1997) or normal to the plate surface as straight-through holes (Kobayashi et al. 2002). In the former case, the channels are sealed by a cover glass slip and the droplets are formed in a well behind the MCs. In the latter case, ~1 mm gap is allowed between the MC plate and cover slip to form a channel for cross-flowing continuous phase. The driving force for droplet formation in MC



Vladisavljević, G.T., Kobayashi, I. and Nakajima, M (2011) Microfluid Nanofluid 10: 1999–1209

emulsification is a difference in Laplace pressure across the oil/water interface in the well and inside a MC. Therefore, the distorted dispersed phase is spontaneously transformed into spherical droplets by interfacial tension (Sugiura et al. 2002a). The role of cross flow is to remove generated droplets from the module and not to control the droplet size. In the dripping regime the droplet size is virtually independent on the flow rate of the dispersed and continuous phase. In contrast, in shear-based systems such as flow focusing devices and T-junctions, flow rates of all phases have a strong effect on the droplet size and have to be precisely controlled at each DFU. As a consequence, shear-based droplet generators are much more difficult to scale up.

Grooved MC arrays for blood rheology measurements were developed by Kikuchi et al. (1992) and optimized for production of uniform droplets by Kawakatsu et al. (1997). Dead-end modules with grooved MC arrays provide a low dispersed phase flow rate of less than 0.1 mL $h^{-1}$ for edible O/W emulsions (Table A2), due to limited number of MCs (100–1,500). Cross-flow grooved MC modules are more suited for higher throughputs and a flow rate of soybean oil of 1.5 mL $h^{-1}$ has been achieved in a cross-flow module consisted of 12,000 microgrooves arranged in 14 parallel arrays (Kobayashi et al. 2010).

Straight-through MC plates have the highest potential for scale-up and a module with $2\times10^5$ symmetric MCs and a throughput of 20–30 mL $h^{-1}$ for triglyceride O/W emulsions have been developed (Kobayashi et al. 2005a) (Table A3). Symmetric MCs are of the same size and geometry (e.g. either circular or rectangular) along the whole cross section of the plate. Rectangular MCs can provide better performance than circular MCs and an aspect ratio of the MC should be at least 3–3.5 to ensure production of highly uniform droplets (Kobayashi et al.



Vladisavljević, G.T., Kobayashi, I. and Nakajima, M (2011) Microfluid Nanofluid 10: 1999–1209

2004). Van Dijke et al. (2010) have confirmed through CFD simulations that a minimal aspect ratio was necessary to allow penetration of the continuous phase inside the MC during droplet detachment. They have found that at the aspect ratio below 3, the growing droplet occupied completely the cross section of the channel, preventing inflow of the continuous phase to the point of snap-off.

Asymmetric MCs have a different shape on different sides of the plate, e.g. cylindrical shape on the upstream side and rectangular shape on the downstream side (Kobayashi et al. 2005b) (Figures 1a and 1b). Asymmetric structure is especially suited for generation of uniform droplets from liquids with a viscosity below 1 mPa s, such as volatile hydrocarbons (C6-C10), e.g. decane (Kobayashi et al. 2005b). Asymmetric straight-through MCs have also been used for production of W/O emulsions (Kobayashi et al. 2009) and polyunsaturated fatty acids (PUFA)-loaded O/W emulsions (Neves et al. 2008).

The maximum throughputs in asymmetric MC array devices have not yet been systematically investigated. The aim of this work is to investigate experimentally and through CFD the effect of dispersed phase viscosity on the maximum flux and maximum droplet generation frequency in asymmetric straight-through MC emulsification.

## 2 Materials and methods

### 2.1 Chemicals

2 wt% Tween 20 (polyoxyethylene (20) sorbitan monolaurate) or 0.01-2 wt% SDS (sodium dodecyl sulphate) dissolved in Milli Q water was used as a continuous phase liquid in O/W emulsions. Both emulsifiers were purchased from Wako Pure Chemical Industries, Ltd, Osaka, Japan. The dispersed phase was soybean oil, MCT (medium-chain fatty acid triglyceride) oil or n-tetradecane with a viscosity at 298 K of 50, 20, and 2.7 mPa·s, respectively (Table 1). The MCT oil containing triglycerides with 6−12 carbon atoms in each fatty acid chain was supplied by Taiyo Kagaku Co. Ltd, Yokkaichi, Japan. Soybean oil and n-tetradecane were purchased from Wako Pure Chemical Industries, Ltd, Osaka.

### 2.2 Silicon chip

The experiments have been carried out using silicon 24 × 24 mm MC plate (model WMS1-3, manufactured by EP. Tech Co., Ltd., Hitachi, Japan) containing 23,348 MCs arranged within a 10×10 mm square region in the centre of the plate. As shown in Figure 1c, the MC plate was 500 μm thick, but it was etched down to thickness 100 μm in the central region. The plate was microfabricated by photolithography and deep reactive ion etching. Each MC consisted of a cylindrical 10-μm diameter straight microhole with a depth of 70 μm and a 50 × 10 μm microslot with a depth of 30 μm (Figure 1b). The slot aspect ratio of 5 was above the threshold value of 3 required for monodisperse emulsion generation. The distance between the centres of adjacent MCs in the vertical rows was 70 μm and the distance between the



Vladisavljević, G.T., Kobayashi, I. and Nakajima, M (2011) Microfluid Nanofluid 10: 1999–1209

centres of MCs in the adjacent rows was 60 μm (Figure 1d). Before first usage, the MC plate was subjected to plasma oxidation in a plasma reactor (PR41, Yamato Science Co. Ltd., Tokyo, Japan) to form a hydrophilic silicon dioxide layer on the surface. After each experiment the plate was gently cleaned in an ultrasound water bath (VS-100 III, As One Co., Osaka, Japan) using a commercial neutral detergent solution and stored in 0.1 M nitric acid solution to maintain its hydrophilicity.

## 2.3 Experimental procedure

Prior to each experiment, MC plate was degassed in the continuous phase by ultrasound treatment for 20 min. The dispersed phase was injected through the MC plate at the flow rate ranging from 1 to 350 mL $h^{-1}$ by a Harvard Apparatus, model 11 Plus or PHD 22/2000 syringe pump. The droplets were removed from the module by the continuous phase delivered from an elevated reservoir through the gap between the MC plate and cover slip (Figure 2). Under laminar flow conditions in the gap ($Re$<500), the shear stress $\tau$ at the MC plate surface is given by: $\tau = 3Q_c\eta_c/(2h^2W)$, where $h$=1 mm is the gap height and $W$=12 mm is the gap width. The meaning of symbols which are not explained explicitly can be found in the nomenclature. The continuous phase flow rate was 50 mL $h^{-1}$ at the minimum dispersed phase flow rate of 1 mL $h^{-1}$ and increased in proportion to the dispersed phase flow rate. $\tau$ had a negligible value of $1.7\times10^{-3}$ Pa at $Q_c$=50 mL $h^{-1}$, and even at $Q_c$=17,500 mL $h^{-1}$ it was only 0.6 Pa. As a comparison, in membrane emulsification the shear stress at the membrane surface is typically in the range of 1–30 Pa (Vladisavljević and Schubert 2003a). As mentioned above, the driving force for droplet detachment in MC emulsification is not a shear stress at the plate surface but a difference in Laplace pressure. The droplet generation was



Vladisavljević, G.T., Kobayashi, I. and Nakajima, M (2011) Microfluid Nanofluid 10: 1999–1209

recorded at 600 frames per second using a Rabitt model mini 2 high-speed camera (Photoron, Tokyo) attached to an inverted metallographic microscope (MS-511-M; Seiwa Optical Co., Ltd., Tokyo), as shown in Figure 2. The droplet generation rate was estimated from the recorded videos. The particle size distribution of the resultant emulsions was measured using a commercial light scattering instrument (Beckman Coulter LS 13 320, Miami, FL). This instrument incorporates Polarization Intensity Differential Scattering technology to provide a measurement range from 0.04 to 2,000 μm with a resolution of 116 particle size channels. The mean droplet size was expressed in terms of the Sauter mean diameter, $d_{3,2}$, which is the diameter of a droplet having the same area per unit volume as that of the total collection of droplets in the emulsion.

## 3 Results and Discussion

### 3.1 CFD simulation

A commercial Computational Fluid Dynamics (CFD) finite volume code (CFD-ACE+ version 2004) was used to predict droplet generation behaviour in a single asymmetric MC for different oils and the results are given in Figure 3. The interfacial tensions used in CFD simulations are the values at the interface between the oil and pure water (Table 1). Thus, it was supposed that during droplet detachment process the surfactant molecules did not have sufficient time to adsorb at oil/water interface in any appreciable amount. It is in agreement with our experimental results obtained on the same MC plate that showed no difference in the droplet size distribution for 2% SDS and 0.01 % SDS in the continuous phase (Vladisavljević et al. 2008). At the oil velocity in the MC of less than 1 mm $s^{-1}$, the droplet diameter was



Vladisavljević, G.T., Kobayashi, I. and Nakajima, M (2011) Microfluid Nanofluid 10: 1999–1209

virtually constant ($d$ = 26.3–27.5 μm) for the investigated oil types. At the critical velocity corresponding to the boundary between dripping and blow-up regime, the droplet diameter sharply increases and the droplet generation frequency reaches a maximum value. At $U < U_{cr}$ the net droplet detaching force (the sum of viscous and buoyancy force) can be neglected compared to the interfacial tension force (Sugiura et al. 2002a) and the droplet diameter is lower than 30 μm. At $U > U_{cr}$ the net droplet detaching force dominates over the interfacial tension and the dispersed phase flows out continuously forming a big droplet ($d$ > 30 μm) at the channel outlet. In the dripping (size-stable) regime the droplet size is controlled by the MC geometry. In the blow-up (continuous outflow) regime, the droplet size is independent of the MC geometry and highly depends on the dispersed phase velocity in the MC. This dependence can be expressed in terms of Capillary number, $Ca = \eta_d U/\gamma$ for laminar conditions and Weber number, $We = \rho_d d U^2/\gamma$ for turbulent conditions. In most cases, flow in MCs is laminar and $Ca$ is used instead of $We$. As shown in Figure 4, the critical velocity for the investigated oils varies from 4 mm $s^{-1}$ for soybean oil to 92 mm $s^{-1}$ for tetradecane. The difference in critical velocity can be explained by a higher viscosity and lower interfacial tension of soybean oil as compared to tetradecane (Table 1), and thus for soybean oil the viscous force exceeds the interfacial tension force at much lower velocity. The Capillary number at the critical velocity was $6\times10^{-3}$ and $7\times10^{-3}$ for tetradecane and soybean oil, respectively. Both capillary numbers are similar, which agrees well with the results reported by Sugiura et al (2002b) and a small discrepancy can be explained by a higher buoyancy force acting on tetradecane droplets.

Figure 4 shows that on a log-log scale the maximum droplet generation frequency per channel linearly increases with decreasing the oil viscosity and ranges from 21 Hz for soybean oil to



Vladisavljević, G.T., Kobayashi, I. and Nakajima, M (2011) Microfluid Nanofluid 10: 1999–1209

440 Hz for n-tetradecane. The maximum droplet generation frequency would continue to increase with the further decrease in oil viscosity until a minimum viscosity ratio is reached, at which droplet formation is no longer possible, as pointed out by van Dijke et al. (2010). The minimum viscosity ratio $\eta_d/\eta_c$ is a function of MC design. In Figure 4, $\log(U_{cr})$ is proportional to $[\log(\eta_d)]^{-1.04}$ and $\log(f_{cr})$ is proportional to $[\log(\eta_d)]^{-1.06}$. Therefore, both $U_{cr}$ and $f_{cr}$ are inversely proportional to $\eta_d$. The maximum droplet generation frequency for soybean oil of 21 Hz predicted here is lower than 30 Hz reported by Kobayashi et al. (2008a) for symmetric MC plate (Table A3). The reason for the discrepancy between 30 Hz achieved by Kobayashi et al. (2008a) and 21 Hz predicted here is in the size of MCs (10×50 μm in this work and 1×5 μm in the previous work). The maximum droplet generation frequency decreases with increasing the channel size, due to increase in the mean droplet size.

### 3.2 Experimental investigations

#### 3.2.1 Mean droplet size and droplet size distribution

Figure 5 illustrates the Sauter mean diameter and the span of particle size distribution for MCT oil-in-water emulsions as a function of flux through the MC plate. In the flux range from zero to 150 L $m^{-2}$ $h^{-1}$ (the size-stable zone) the mean particle size was virtually constant ($d_{3,2}$ = 27.1–27.6 μm) with a span of 0.20–0.23. The same type of behaviour was observed for a grooved terrace-based MC system (Sugiura at al. 2002b). In the size-stable zone (a) the particle sizes occupy just three size channels of the particle size analyser (Figure 6a), which indicates very high degree of droplet size uniformity. Such low span values cannot normally be obtained in membrane emulsification, as shown in Table A1. In the flux range from 150 to 600 L $m^{-2}$ $h^{-1}$ the Sauter mean diameter expanded from 27.6 to 31.2 μm and the droplets



Vladisavljević, G.T., Kobayashi, I. and Nakajima, M (2011) Microfluid Nanofluid 10: 1999–1209

remained uniform with a span of 0.20–0.25. Therefore, quasi-monodispersed droplets were formed at the flux below 600 L $m^{-2}$ $h^{-1}$, therefore in both size-stable and size-expanding zone. The size stable and size-expanding zone can be distinguished by the numerical value of the slope and the correlation coefficient $R$ between $d_{3,2}$ and $J$. Within size-stable zone $R^2$ is typically between 0.1 and 0.6 and within size-expanding zone $R^2$ is above 0.9. In addition, the slope of $d_{3,2}$ vs. $J$ in size-stable region is much smaller than that in size-expanding zone. In Figure 5, $R^2$=0.15 within the size-stable zone and $R^2$=0.93 for the size-expanding zone. In addition, the slope of the $d_{3,2}$ vs. $J$ in the size-expanding zone is about 5 times greater than that in size-stable zone.

The critical flux will be arbitrarily defined as a maximum flux corresponding to the span value of 0.3. Beyond the critical flux, big droplets started to form from some of the MCs, although the majority of the MCs continued to generate small droplets. With the further increase in flux, progressively more MCs have produced big droplets. Because a transition from size-expanding to blow-up regime did not occur simultaneously for all the MCs, the droplets in the blow-up regime were polydisperse with a span of 0.75–0.95 (Figure 6c). Droplet size in this regime is controlled by the balance between the shear force due to cross flow, the viscous force due to dispersed phase flow, the push-off force as a result of contact between the droplets growing at the plate surface (Egidi et al. 2008), etc.

The mean oil velocity $\overline{U}$ in the channels and the oil flux $J$ are related by the equation:

$$\overline{U} = 4JA_m /(\pi d_{ch}^2 kN_0) \quad (1)$$



Vladisavljević, G.T., Kobayashi, I. and Nakajima, M (2011) Microfluid Nanofluid 10: 1999–1209

where $A_m$ = 1 cm$^2$ is the cross sectional area of the square central region of the MC plate, $d_{ch}$ = 10 μm is the MC diameter, $k$ is the fraction of active MCs, and $N_0$ = 23,348 is the number of MCs in the plate. In the size stable zone at $J$ < 150 L m$^{-2}$ h$^{-1}$, one obtains from Eq. (1) that $\overline{U}$ < 2.3 mm s$^{-1}$ for $k$ = 1, which agrees well with the CFD results for MCT oil in Figure 3. According to Eq. (1), the average velocity in the MCs in the size-expanding zone is 2.3–9.1 mm s$^{-1}$. The experimental value for the critical velocity of MCT oil of 9.1 mm s$^{-1}$ is in good agreement with 9.8 mm s$^{-1}$, obtained from CFD simulation (Figure 4).

Figure 7a shows the effect of tetradecane flux through the MC plate on the mean particle size and the distribution span. At the flux below 900 L m$^{-2}$ h$^{-1}$ the Sauter mean diameter $d_{3,2}$ was virtually independent on tetradecane flux and the span was in the range of 0.23–0.49. Thus, in the size-stable zone the resultant tetradecane droplets were less uniform than MCT oil droplets. The maximum span of 0.49 was obtained for the minimum tetradecane flux of 10 L m$^{-2}$ h$^{-1}$, which can be explained by a low pressure droplet in the MCs due to relatively low tetradecane viscosity. Sugiura et al. (2002b) have found that a large pressure droplet across the channel may help to obtain more stable and uniform droplet generation due to internal disturbances of the flow within a channel. Regardless of the relatively high span value for tetradecane droplets at 10 L m$^{-2}$ h$^{-1}$, the collected droplets are uniform in size when observed under optical microscope, with no satellite or big droplets, as shown in Figure 7b.

A narrow particle size distribution with a span in the range of 0.22–0.32 persisted to 2700 L m$^{-2}$ h$^{-1}$. At the critical flux of 2700 L m$^{-2}$ h$^{-1}$ the overall throughput was 3.2×10$^6$ droplets per second, the Sauter mean diameter of the resultant droplets was 35.6 μm and the span value was 0.30. A transition from size-expanding to blow-up regime was very gradual, so even at

the flux of 3500 L $m^{-2}$ $h^{-1}$ the span was only 0.41. The fraction of active channels, $k$ was about 0.5 at the critical tetradecane flux. By putting $k$ = 0.5 (from experimental observations) and $\overline{U}$ = 92 mm $s^{-1}$ (from CFD analysis, Fig. 4) in Eq. (1), one obtains the critical flux $J_{cr}$ = 3040 L $m^{-2}$ $h^{-1}$. This value deduced from CFD is higher than 2700 L $m^{-2}$ $h^{-1}$ estimated from Figure 7a. The deviation of 10% between the experimental and CFD value for $J_{cr}$ can be explained by a very gradual transition from the size-expanding to blow-up regime and thus, a boundary between the two regimes cannot be determined with great certainty. The experimental results shown in Fig. 5 and 7a confirm the CFD findings that the critical velocity is lower when the viscosity of the disperse phase is higher.

Figure 8 shows the effect of soybean oil flux on the Sauter mean diameter and the size distribution span for the experiments performed in the flux range between 0–120 L $m^{-2}$ $h^{-1}$. The droplets were highly uniform (span = 0.21–0.24) over the investigated range of flux and the blow up regime was not reached at 120 L $m^{-2}$ $h^{-1}$. It is not surprising, because the critical flux calculated from Eq. (1) is 260 L $m^{-2}$ $h^{-1}$ and the critical velocity in MC is 4 mm $s^{-1}$, which is the well above the maximum channel velocity applied here. The Sauter mean diameter was 25.5±0.3 μm in the size-stable zone (0–50 L $m^{-2}$ $h^{-1}$) and increased to 27.4 μm in the size-expanding zone. Because the maximum channel velocity applied in the experiments shown in Fig. 8 was below the critical velocity, the blow-up regime was not identified.

3.2.2 Droplet formation frequency and fraction of active pores



Vladisavljević, G.T., Kobayashi, I. and Nakajima, M (2011) Microfluid Nanofluid 10: 1999–1209

Mean droplet formation frequency was estimated from high speed video recordings by counting the number of droplets produced from a given channel within a certain time period. At least 50 different active channels were observed at each set of experimental conditions. At the tetradecane flux of above $10^3$ L $m^{-2}$ $h^{-1}$, more than 2 millions droplets per second were produced in the module and due to such high droplet productivity, only channels at the upstream edge of the plate were accessible to observation. At the lower fluxes, the observed channels were randomly chosen from the entire MC plate. Although the mean droplet formation frequency in repeated measurements conducted under the same conditions was relatively stable, as shown in Figure 9, channel to channel variations over the plate surface were significant, with a coefficient of variation of 20–50%. For example, at the tetradecane flux of 10 L $m^{-2}$ $h^{-1}$ the mean droplet formation frequency $\bar{f}$ was 17 Hz, but the $f$ values for individual active channels randomly varied over the plate from 8 to 35 Hz. Significant channel to channel variations in the droplet generation frequency even for the channels at a small distance from each other can be seen in Figure 10a. The tetradecane droplets arising from different channels were of equal size, but the frequency of their generation varied from channel to channel, which can be seen from variable distance between the adjacent droplets in different droplet streams. For example, the droplet generation frequency for droplet stream 1 and 2 was considerably higher than that for that for streams 5 and 6.

Frequency of droplet generation determined by CFD and experimentally is plotted as a function of Capillary number, $Ca$ in Figure 11. $\gamma$ in the equation for $Ca$ ($=\eta_d \overline{U} / \gamma$) was assumed to be the interfacial tension at the interface between pure water and oil (see Table 1), i.e. the mass transfer of emulsifier to the liquid interface was neglected due to short detachment times. At the constant oil flux, the mean droplet generation frequency was the



Vladisavljević, G.T., Kobayashi, I. and Nakajima, M (2011) Microfluid Nanofluid 10: 1999–1209

highest for n-tetradecane and the lowest for soybean oil. The reason for this behavior was explained in the next paragraph. The agreement between the experimental and CFD data was rather good, especially for soybean oil. The mean droplet generation frequency $\bar{f}$ for tetradecane reached 250 Hz at the critical flux, which is lower than 440 Hz, predicted by CFD analysis. Although droplet generation frequency for individual channels can reach a theoretical maximum of 440 Hz, the mean value is significantly lower due to large channel to channel variations in *f*.

The mean droplet generation rate is closely related to the fraction of active channels, *k*, which can be calculated from the mass balance equation for dispersed phase:

$$k = 6JA/(d_{4,3}^3 \pi \bar{f} N_0) \qquad (2)$$

where $d_{4,3}$ is the volume weighted mean particle diameter, which is the sum of the volume ratio of droplets in each size class multiplied by the mid-point diameter of the size class (McClements, 2004). Figure 9 shows that the mean droplet generation frequency increases with increasing tetradecane flux, but at a decreasing rate. Therefore, fraction of active channels should increase with flux, according to Eq. (2). The same conclusion can be derived from microscope images in Figure 10. At 10 L $m^{-2}$ $h^{-1}$ (Figure 10a), only 4 channels were active, out of approximately 100 channels that can be seen in the figure, e.g. the proportion of active MCs was only 4%. On the other hand, at 500 L $m^{-2}$ $h^{-1}$ (Figure 10b) more than 40 % of the MCs were active. The similar results have been obtained by Abrahamse et al. (2002) using a microengineered microsieve membrane with uniform cylindrical pores. At the transmembrane pressure 3 times the critical pressure, they have found that the proportion of active pores was still only 16 %. Lowering and raising the pressure during experiments, they have found that different pores were active in different stages at the same pressure, suggesting



Vladisavljević, G.T., Kobayashi, I. and Nakajima, M (2011) Microfluid Nanofluid 10: 1999–1209

that the pores became active at random. According to Abrahamse et al. (2002), as soon as oil flows through a certain number of pores, the pressure under the membrane on the upstream side is reduced preventing other pores from being activated. At a higher flux more pores become active because the pressure difference increases and thus, the capillary pressure for a given pore is more likely to be overcome by the driving pressure.

Percentage of active channels calculated from the experimental $\bar{f}$ values using Eq. (2) is plotted as a function of dispersed phase flux in Figure 12. The fraction of active channels increased with increasing flux and viscosity of the dispersed phase. For soybean oil, the fraction of active channels increased with increasing flux from 49 % at 10 L $m^{-2}$ $h^{-1}$ to 97 % at 70 L $m^{-2}$ $h^{-1}$ and then remained roughly constant with the further increase in flux. For MCT oil, the fraction of active channels increased from 9 % at 10 L $m^{-2}$ $h^{-1}$ to 90 % at 130 L $m^{-2}$ $h^{-1}$. The higher proportion of active channels for soybean oil as compared to MCT oil and tetradecane can be explained by the higher viscosity of soybean oil leading to a higher upstream pressure and therefore, the capillary pressure for a given channel is more likely to be overcome. For each type of oil, the flux at which channel activation was finished coincided approximately with the flux at a boundary between size-stable and size-expanding zone. Therefore, in size-expanding zone the number of active pores was almost independent on flux.



Vladisavljević, G.T., Kobayashi, I. and Nakajima, M (2011) Microfluid Nanofluid 10: 1999–1209

## 4 Conclusions

The maximum droplet throughput in MC emulsification is strongly affected by the viscosity of the dispersed phase. Monodisperse droplets can only be formed if the interfacial tension force dominates over the sum of the buoyancy and viscous force, the latter being proportional to $U\eta_d$. The lower the dispersed phase visocosity $\eta_d$, the higher the velocity $U$ in the MC at which the interfacial tension force will be overcome and the higher the maximum disperse phase flux that can be achieved. The maximum dispersed phase flux in this work ranged from over 120 L $m^{-2}$ $h^{-1}$ for soybean oil ($\eta_d$ = 50 mPa s) to 2700 L $m^{-2}$ $h^{-1}$ for n-tetradecane ($\eta_d$ = 2.7 mPa s). The droplets of soybean and MCT oil produced in the size-stable and size-expanding regime were highly uniform in size with a distribution span in the range of 0.21–0.25. At the constant flux the droplet generation frequency increased with decreasing viscosity of the dispersed phase because the smaller proportion of microchannels was involved in droplet generation. For n-tetradecane, the maximum mean droplet generation frequency was 250 droplets per second per active channel, corresponding to the overall plate productivity of 3.2 million droplets per second. The fraction of active channels increased with increasing flux and most of the increase has occurred in the size-stable zone. For soybean oil, the fraction of active channels exceeded 95% at the boundary between the size-stable and size expanding regime. For n-tetradecane, due to smaller viscosity the fraction of active channels was only 50% at the boundary between the size-stable and size expanding regime. The correlation between experimental and CFD results was very good, particularly for soybean oil. These results can be applied for optimisation of the internal structure of microporous membranes used in membrane emulsification and for optimisation of microchannel geometry in PDMS microfluidics.



Vladisavljević, G.T., Kobayashi, I. and Nakajima, M (2011) Microfluid Nanofluid 10: 1999–1209

***Acknowledgements*** This work was supported by the Japan Society for the Promotion of Science, Tokyo (the invitation fellowship of Dr Goran Vladisavljević ID No. L-05555) and by the Food Nanotechnology Project of the Ministry of Agriculture, Forestry and Fisheries of Japan.

**References**

Abate AR, Weitz DA (2009) High-order multiple emulsions formed in poly(dimethylsiloxane) microfluidics. Small 18:2030–2032

Abrahamse AJ, van Lierop R, van der Sman RGM,van der Padt A, Boom RM (2002) Analysis of droplet formation and interactions during cross-flow membrane emulsification. J Membr Sci 204:125–137

Anna SL, Bontoux, N, Stone HA (2003) Formation of dispersions using 'flow-focusing' in microchannels. Appl Phys Lett 82:364–366

Egidi E, Gasparini G, Holdich RG, Vladisavljević GT, Kosvintsev SR (2008) Membrane emulsification using membranes of regular pore spacing: Droplet size and uniformity in the presence of surface shear. J Membr Sci 323:414–420

Holdich RG, Dragosavac MM, Vladisavljević GT, Kosvintsev SR (2010) Membrane emulsification with oscillating and stationary membranes. Ind Eng Chem Res 49:3810–3817

Kawakatsu T, Kikuchi Y, Nakajima M (1997) Regular-sized cell creation in microchannel emulsification by visual microprocessing method. J Am Oil Chem Soc 74:317–321

Kikuchi Y, Sate K, Ohki H, Kaneko T (1992) Optically accessible microchannels formed in a single-crystal silicon substrate for studies of blood rheology. Microvasc Res 44:226–240

Kobayashi I, Nakajima M, Chun K, Kikuchi Y, Fujita H (2002) Silicon array of elongated through-holes for monodisperse emulsion droplets. AIChE J 48 (2002) 1639–1644

Kobayashi I, Nakajima M, Mukataka S (2003) Preparation characteristics of oil-in-water emulsions using differently charged surfactants in straight-through microchannel emulsification. Colloids Surf A: Physicochem Eng Aspects 229:33–41

Kobayashi I, Mukataka S, Nakajima M (2004) Effect of slot aspect ratio on droplet formation from silicon straight-through microchannels. J Colloid Interface Sci 279:277–280

Kobayashi I, Mukataka S, Nakajima M (2005a) Production of monodisperse oil-in-water emulsions using a large silicon straight-through microchannel plate. Ind Eng Chem Res 44:5852–5856

Kobayashi I, Mukataka S, Nakajima M (2005b) Novel asymmetric through-hole array microfabricated on a silicon plate for formulating monodisperse emulsions. Langmuir 21:7629–7632

Kobayashi I, Uemura K, Nakajima M (2007) Formulation of monodisperse emulsions using submicron-channel arrays. Colloids Surf A: Physicochem Eng Aspects 296:285–289

Kobayashi I, Takayuki T, Maeda R, Wada Y, Uemura K, Nakajima M (2008a) Straight-through microchannel devices for generating monodisperse emulsion droplets several microns in size. Microfluid Nanofluid 4:167–177

Kobayashi I, Wada Y, Uemura K, Nakajima M (2008b) Generation of uniform drops via through-hole arrays micromachined in stainless-steel plates. Microfluid Nanofluid 5:677–687

Kobayashi I, Wada Y, Uemura K, Nakajima M (2009) Production of monodisperse water-in-oil emulsions consisting of highly uniform droplets using asymmetric straight-through microchannel arrays. Microfluid Nanofluid 7:107–119

Kobayashi I, Wada Y, Uemura K, Nakajima M (2010) Microchannel emulsification for mass production of uniform fine droplets: integration of microchannel arrays on a chip. Microfluid Nanofluid 8:255–262

Link DR, Anna SL, Weitz DA, Stone HA (2004) Geometrically mediated breakup of drops in microfluidic devices. Phys Rev Lett 92:054503

McClements DJ (2004) Food Emulsions: principles, practices, and techniques. CRC Press, Boca Raton

Nakashima T, Shimizu M, Kukizaki M (2000) Particle control of emulsion by membrane emulsification and its applications. Adv Drug Deliv Rev 45:47–56

Neves MA, Ribeiro HS, Fujiu KB, Kobayashi I, Nakajima M (2008) Formulation of controlled size PUFA-loaded oil-in-water emulsions by microchannel emulsification using $\beta$-carotene-rich palm oil. Ind Eng Chem Res 47: 6405–6411

Nisisako T, Torii T, Takahashi T, Takizawa Y (2006) Synthesis of monodisperse bicolored Janus particles with electrical anisotropy using a microfluidic co-flow system. Adv Mater 18: 1152–1156

Nisisako T, Torii T (2006) Microfluidic large-scale integration on a chip for mass production of monodisperse droplets and particles. Lab Chip 8:287–293

Steegmans ML, Schroën KGPH, Boom RM (2009) Characterization of emulsification at flat Y junctions. Langmuir 25:3396–3401

Sugiura S, Nakajima M, Kumazawa N, Iwamoto S, Seki M (2002a) Characterization of spontaneous transformation-based droplet formation during microchannel emulsification. J Phys Chem B 106:9405–9409

Sugiura S, Nakajima M, Seki M (2002b) Effect of channel structure on microchannel emulsification. Langmuir 18:5708–5712

Thorsen T, Roberts RW, Arnold FH, Quake SR (2001) Dynamic pattern formation in a vesicle-generating microfluidic device. Phys Rev Lett 86:4163–4166

Utada AS, Lorenceau, E, Link, DR, Kaplan, PD, Stone, HA, Weitz, DA (2005) Monodisperse double emulsions generated from a microcapillary device. Science 308:537–541

Utada AS, Chu, LY, Fernandez-Nieves A, Link DR, Holtze C, Weitz DA (2007) Dripping, jetting, drops, and wetting: the magic of microfluidics. MRS Bull 32:702–708

van Dijke KC, Veldhuis G, Schroën K, Boom R (2009a) Simultaneous formation of many droplets in a single microfluidic droplet formation unit. AIChE J 56: 833–836

van Dijke K, Veldhuis G, Schroën K, Boom R (2009b) Parallelized edge-based droplet generation (EDGE) devices. Lab Chip 9: 2824–2830

van Dijke K, Kobayashi I, Schroën K, Uemura K, Nakajima M, Boom R (2010) Effect of viscosities of dispersed and continuous phases in microchannel oil-in-water emulsification. Microfluid Nanofluid 9:77–85

Vladisavljević GT, Schubert H (2003a) Influence of process parameters on droplet size distribution in SPG membrane emulsification and stability of prepared emulsion droplets. J Membr Sci 225:15–23

Vladisavljević GT, Schubert H (2003b) Preparation of emulsions with a narrow particle size distribution using microporous $\alpha$-alumina membranes. J Disper Sci Technol 24:811–819

Vladisavljević GT, Shimizu M, Nakashima T (2006) Production of multiple emulsions for drug delivery systems by repeated SPG membrane homogenization: Influence of mean pore size, interfacial tension and continuous phase viscosity. J Membr Sci 284:373–383

Vladisavljević GT, Williams RA (2006) Manufacture of large uniform droplets using rotating membrane emulsification. J Colloid Interface Sci 299:396–402

Vladisavljević GT, Kobayashi I, Nakajima M (2008) Generation of highly uniform droplets using asymmetric microchannels fabricated on a single crystal silicon plate: Effect of emulsifier and oil types. Powder Technol 183:37–45

Williams RA, Peng SJ, Wheeler DA, Morley NC, Taylor D, Whalley M, Houldsworth DW (1998) Controlled production of emulsions using a crossflow membrane: Part II: industrial scale manufacture. Chem Eng Res Des 76:902–910

Xu Q, Nakajima M (2004) The generation of highly monodisperse droplets through the breakup of hydrodynamically focused microthread in a microfluidic device. Appl Phys Lett 83:3726–3728

Yobas L, Martens S, Ong WL, Ranganathan N (2006) High-performance flow-focusing geometry for spontaneous generation of monodispersed droplets. Lab Chip 6:1073–1079

**Table 1** Physical properties of dispersed phase used in this work

| oil | density at 25 °C kg $m^{-3}$ | viscosity at 25 °C mPa s | refractive index | interfacial tension* mN $m^{-1}$ |
|---|---|---|---|---|
| soybean oil | 920 | 50 | 1.47 | 25 |
| n-tetradecane | 763 | 2.7 | 1.43 | 50 |
| MCT oil** | 940 | 20 | 1.45 | 30 |

*In contact with pure water.

**MCT = Medium-chain triglyceride



Vladisavljević, G.T., Kobayashi, I. and Nakajima, M (2011) Microfluid Nanofluid 10: 1999–1209

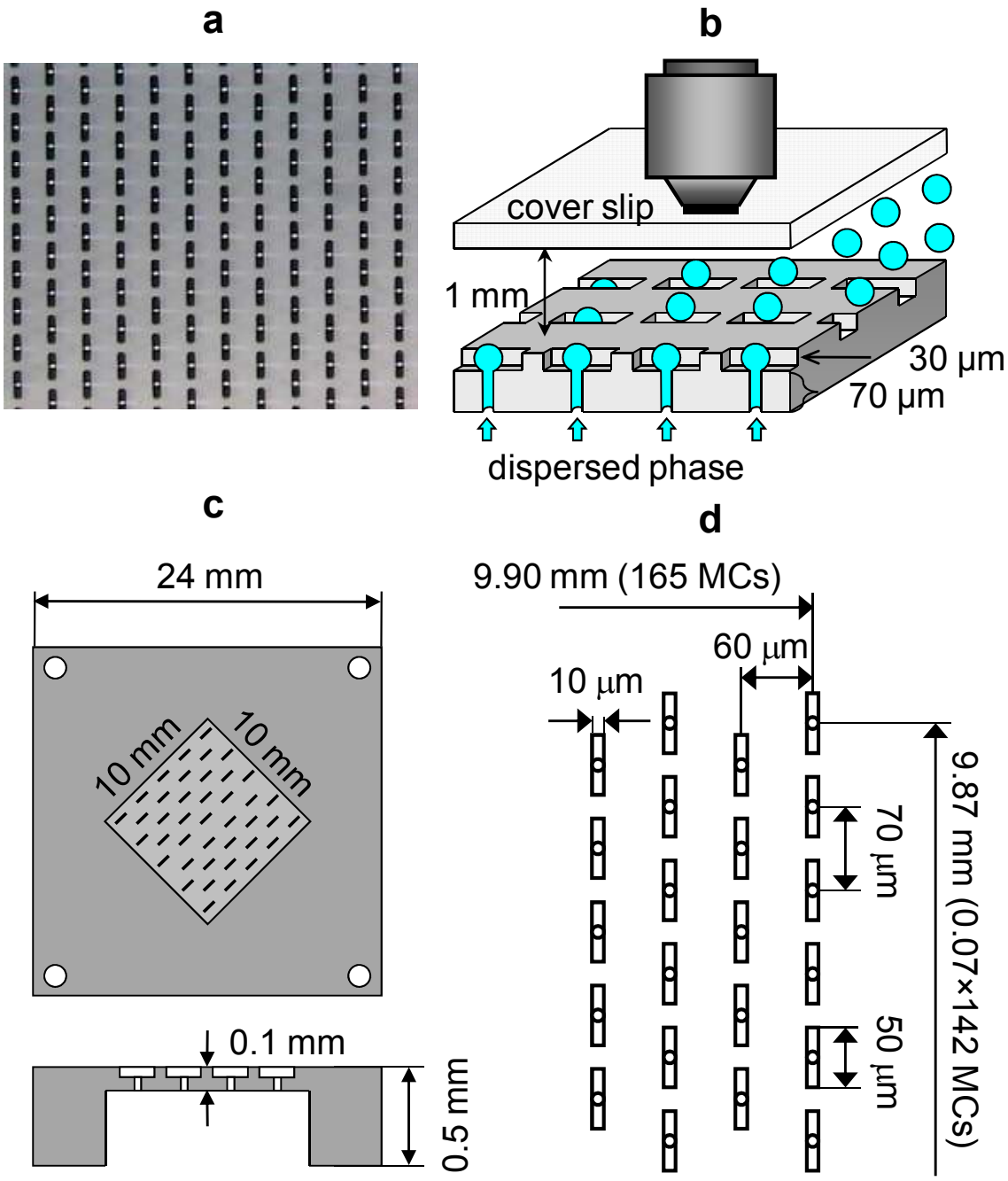


**Fig. 1** **a** Micrograph of the chip surface illuminated from the bottom (upstream) side. Cylindrical holes can be seen as bright dots in the centre of each slot. **b** Schematic view of droplet generation from a fragment of MC plate surface. **c** Schematic representation of the WMS1-3 chip. **d** Array of MCs on the top (downstream) side of the chip. Each vertical row contains alternately 142 and 141 MCs. There are 83 vertical rows with 142 MCs and 82 rows with 141 MCs making the total number of MCs equal to 23,348=83×142+82×141.



Vladisavljević, G.T., Kobayashi, I. and Nakajima, M (2011) Microfluid Nanofluid 10: 1999–1209

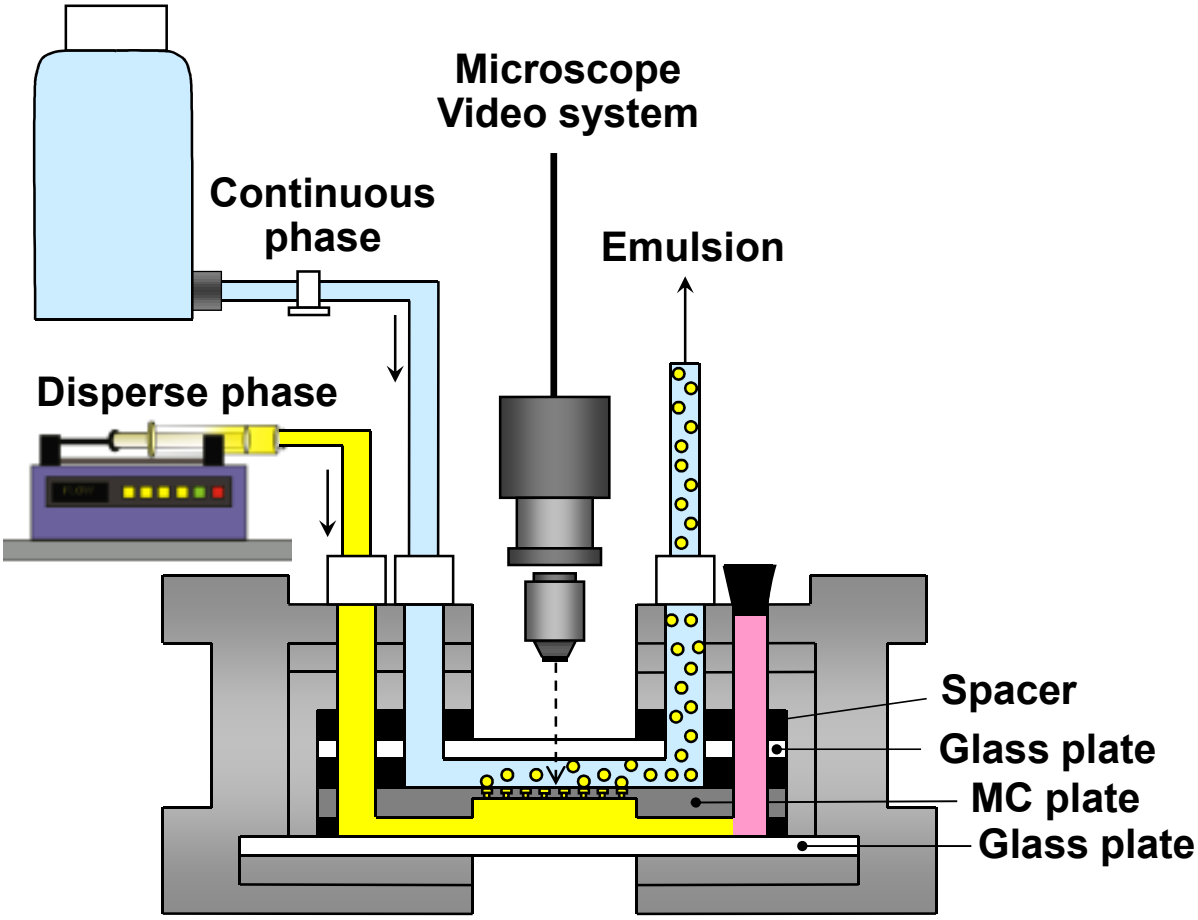


**Fig 2** Simplified schematic diagram of the experimental set-up.



Vladisavljević, G.T., Kobayashi, I. and Nakajima, M (2011) Microfluid Nanofluid 10: 1999–1209

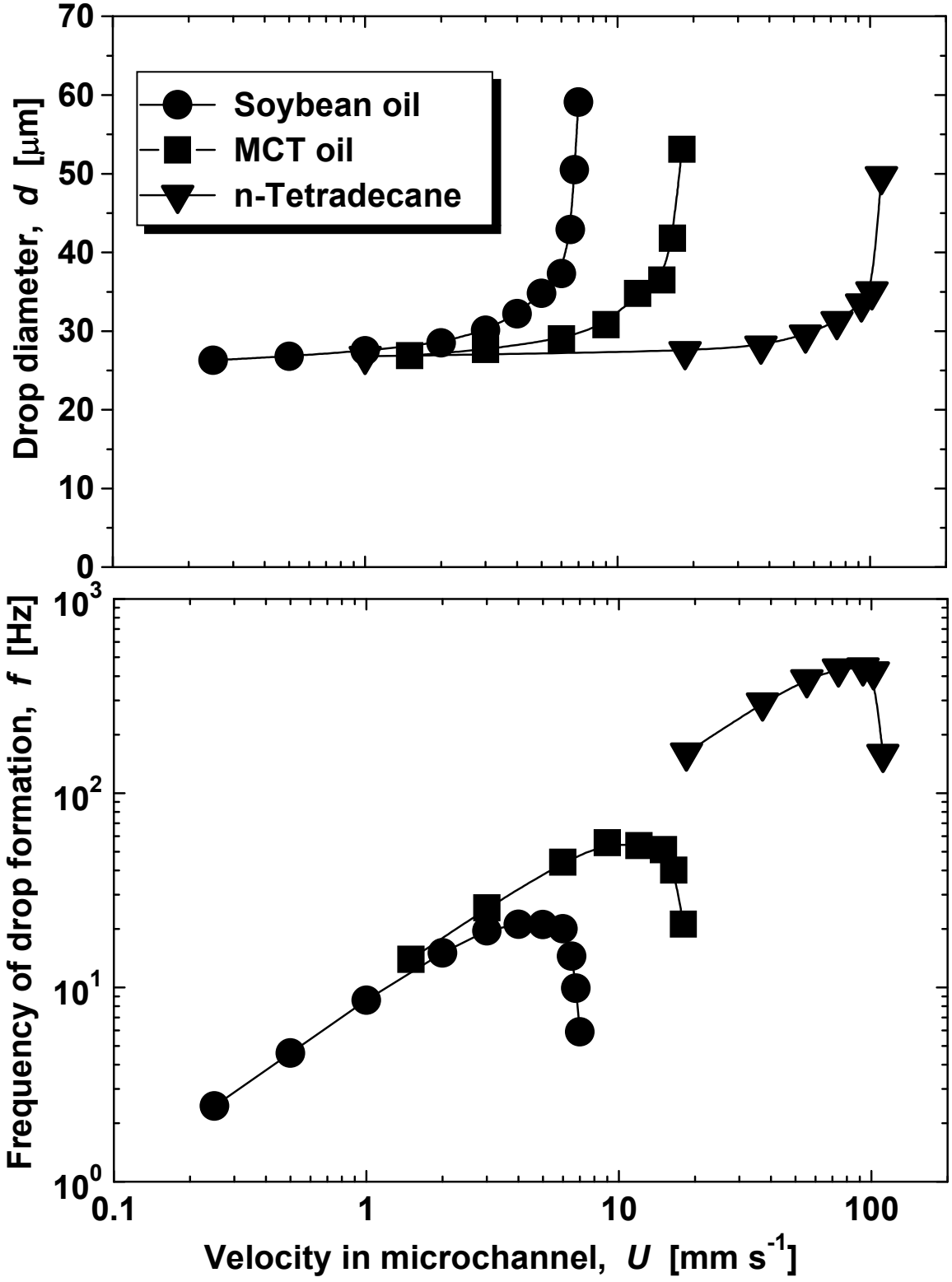


**Fig 3** CFD results showing the effects of oil velocity in an asymmetric MC on the droplet diameter and the frequency of droplet generation. Channel dimensions: 10×10 μm, slot dimensions: 10×50 μm.



Vladisavljević, G.T., Kobayashi, I. and Nakajima, M (2011) Microfluid Nanofluid 10: 1999–1209

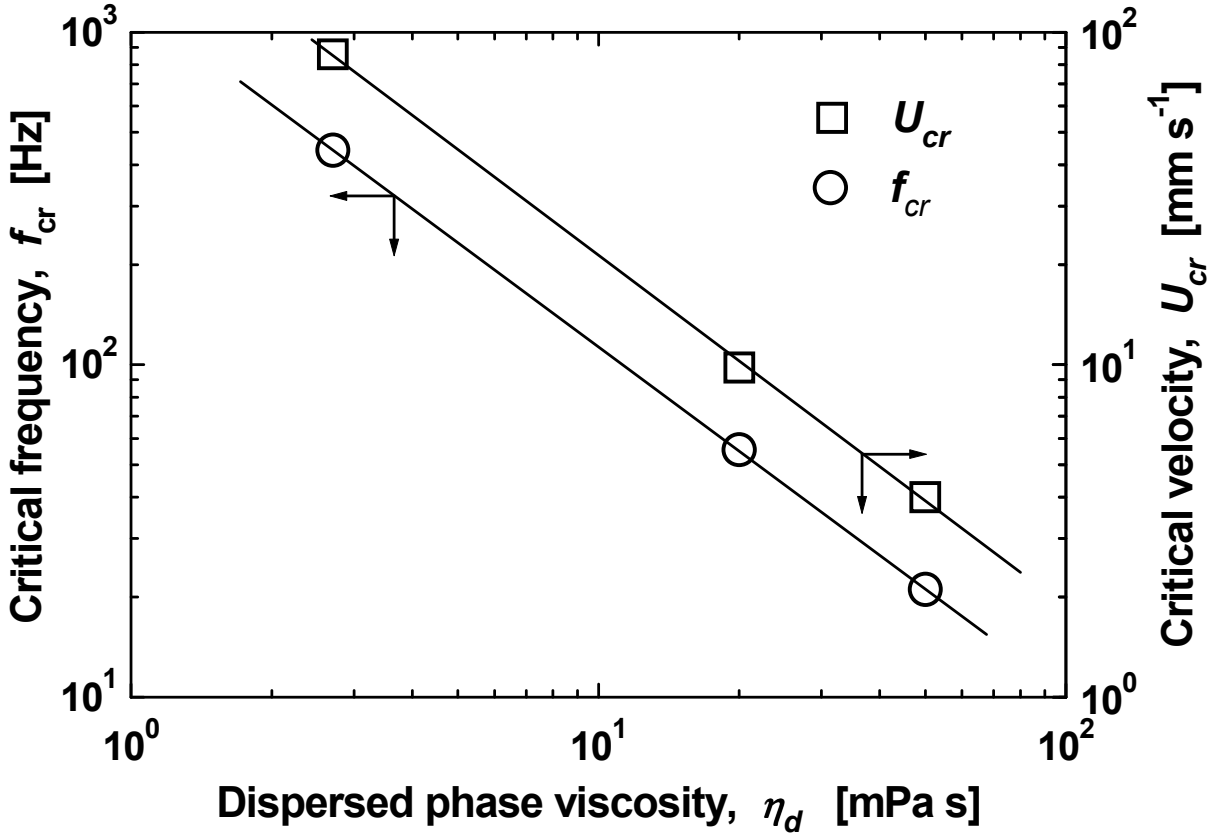


**Fig 4** CFD results showing the critical (maximum) droplet generation frequency from a single asymmetric MC and the critical velocity in MC as a function of the dispersed phase viscosity on a log-log scale. Channel dimensions: 10×10 μm, slot dimensions: 10×50 μm.



Vladisavljević, G.T., Kobayashi, I. and Nakajima, M (2011) Microfluid Nanofluid 10: 1999–1209

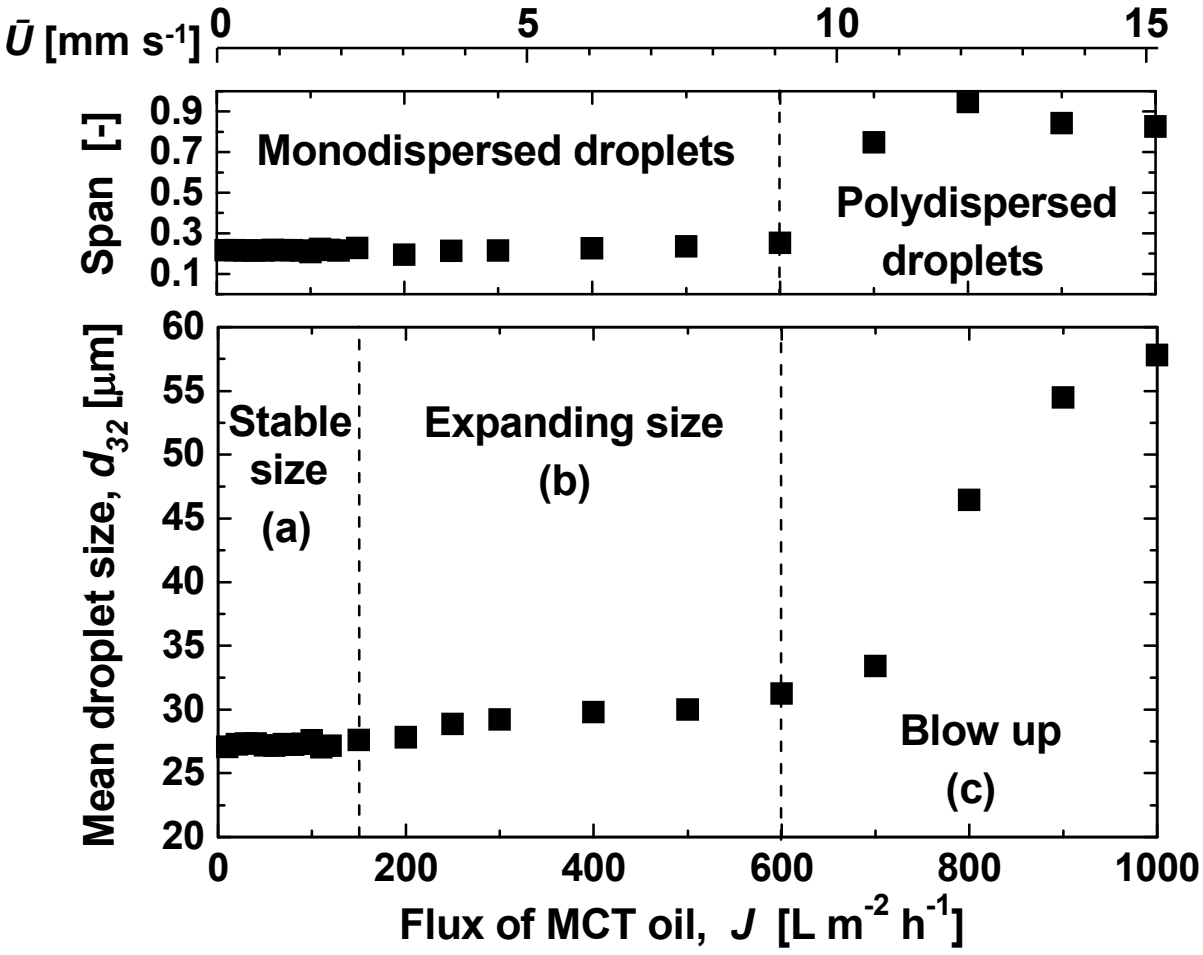


**Fig 5** The effect of the flux of MCT oil on the mean droplet size and a span of particle size distribution. Three different regimes of droplet generation can be clearly distinguished and their boundaries are shown by dashed lines. Monodispersed droplets were formed in the size-stable and size-expending regime.



Vladisavljević, G.T., Kobayashi, I. and Nakajima, M (2011) Microfluid Nanofluid 10: 1999–1209

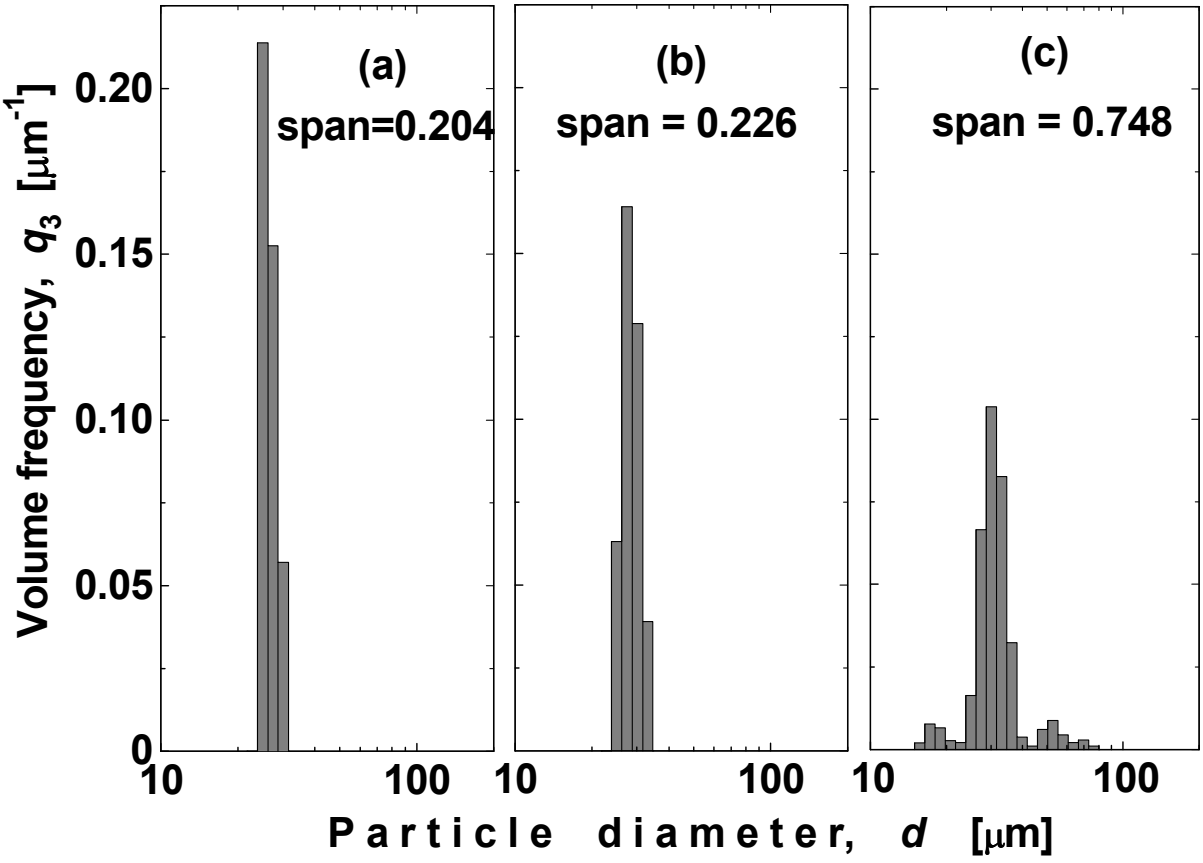


**Fig 6** Typical particle size distribution of MCT oil-in-water emulsions produced in: (a) size-stable regime; (b) size-expanding regime; (c) blow up regime.



Vladisavljević, G.T., Kobayashi, I. and Nakajima, M (2011) Microfluid Nanofluid 10: 1999–1209

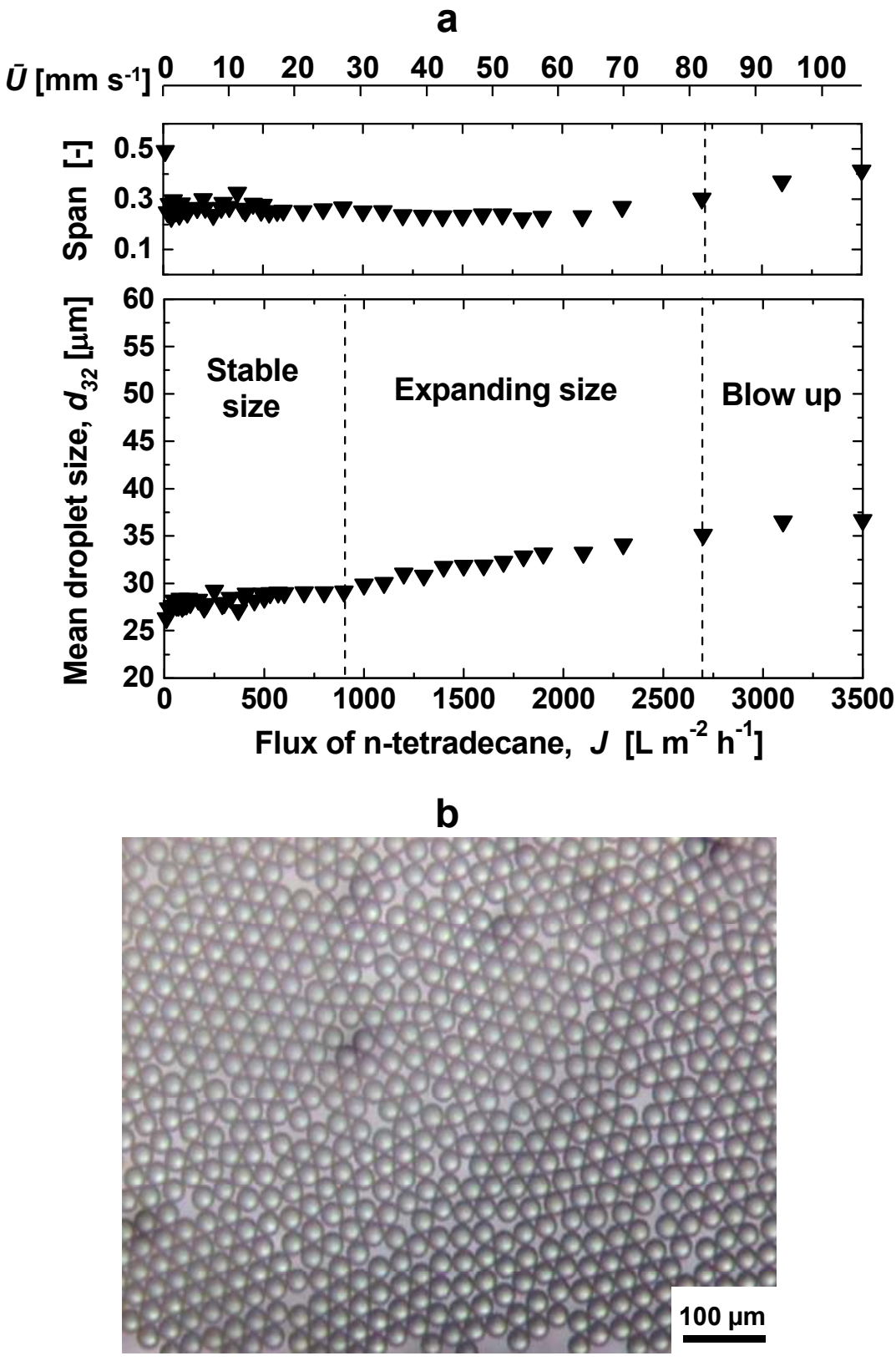


**Fig 7 a** The effect of the flux of n-tetradecane on the mean droplet size and a span of particle size distribution. **b** Optical microscope image of uniform tetradecane droplets with a Sauter mean diameter of 27 μm generated in size-stable regime.



Vladisavljević, G.T., Kobayashi, I. and Nakajima, M (2011) Microfluid Nanofluid 10: 1999–1209

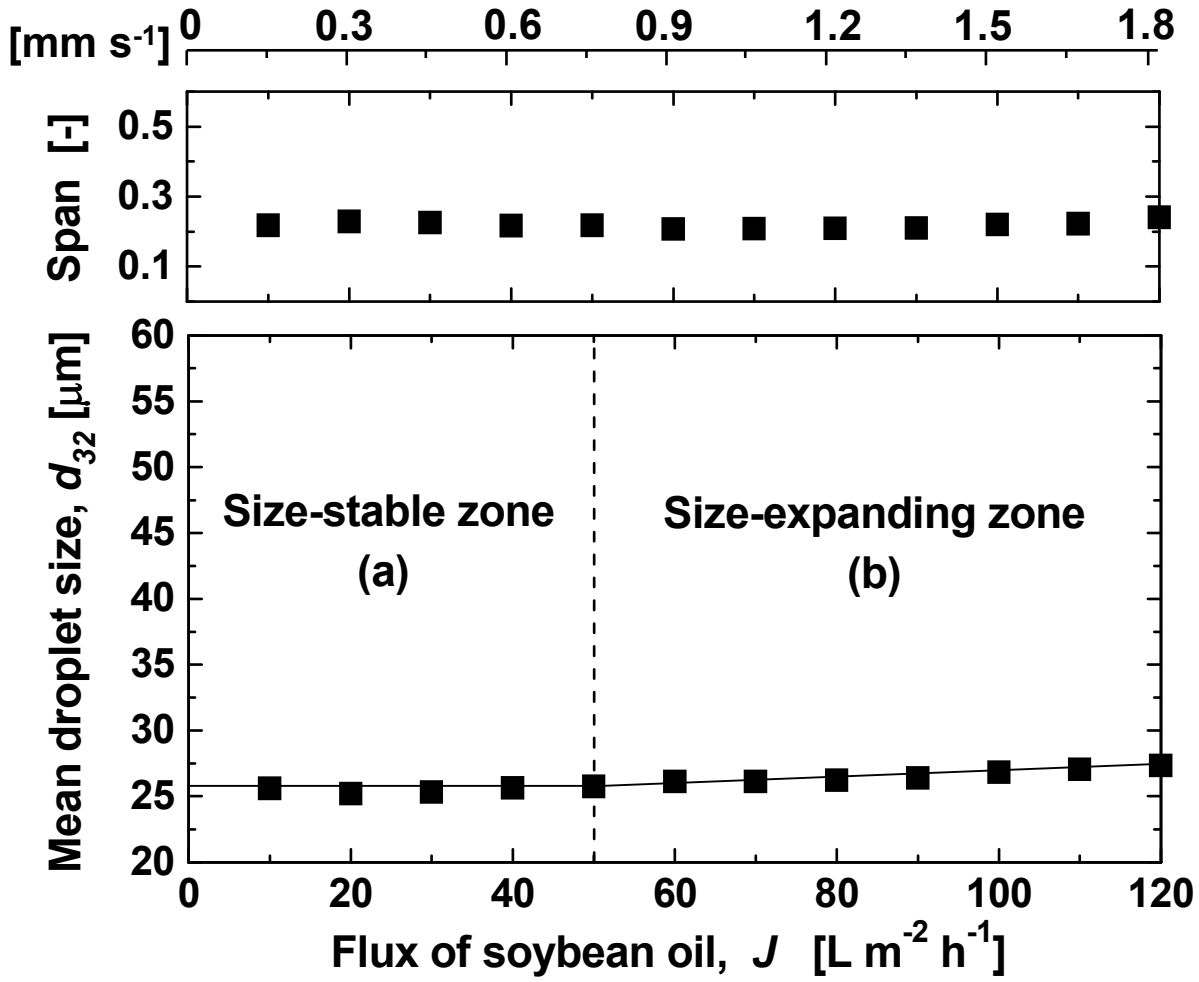


**Fig 8** The effect of the flux of soybean oil on the mean droplet size and a span of particle size distribution.



Vladisavljević, G.T., Kobayashi, I. and Nakajima, M (2011) Microfluid Nanofluid 10: 1999–1209

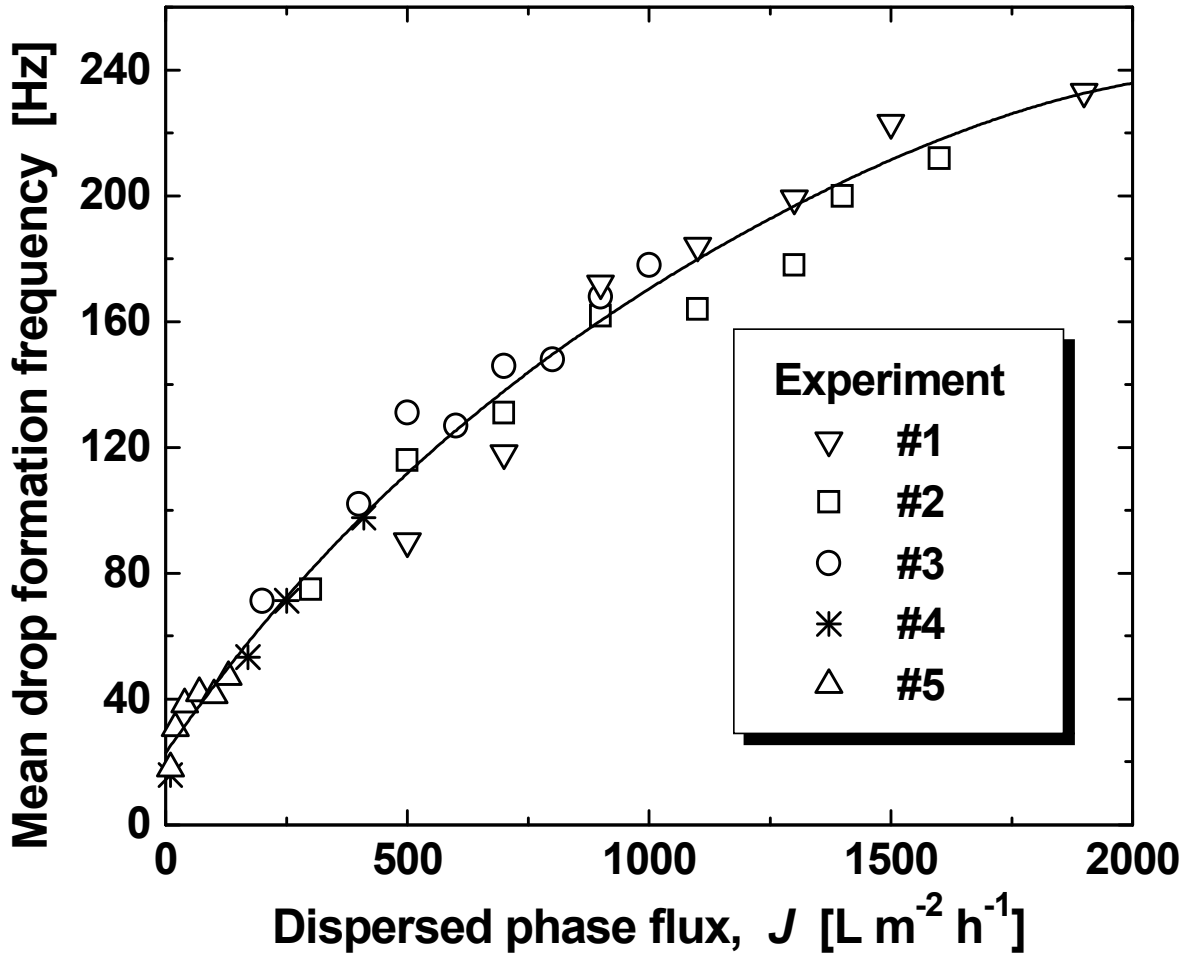


**Fig 9** Reproducibility of the measurements of the mean droplet generation frequency in 5 repeated experiments: Dispersed phase: tetradecane; aqueous phase: 2 wt% Tween 20.



Vladisavljević, G.T., Kobayashi, I. and Nakajima, M (2011) Microfluid Nanofluid 10: 1999–1209

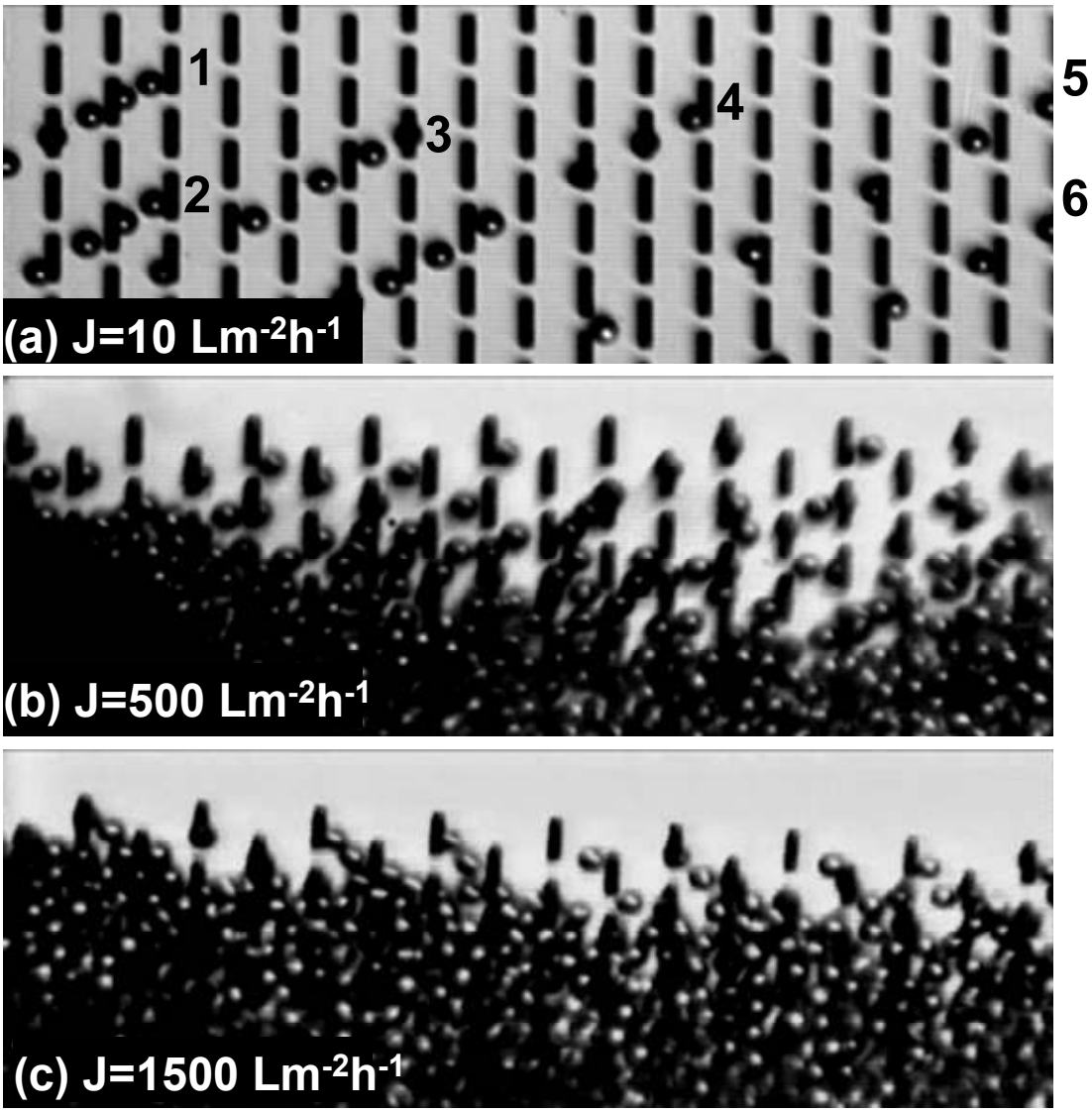


**Fig 10** Microscopic images taken from the high-speed video recordings showing generation of tetradecane droplets at different fluxes (emulsifier: 2 wt% Tween 20). The locations of active channels at 10 L $m^{-2}$ $h^{-1}$ are designated by the numbers 1-6. Channels 5 and 6 are located outside the picture area.



Vladisavljević, G.T., Kobayashi, I. and Nakajima, M (2011) Microfluid Nanofluid 10: 1999–1209

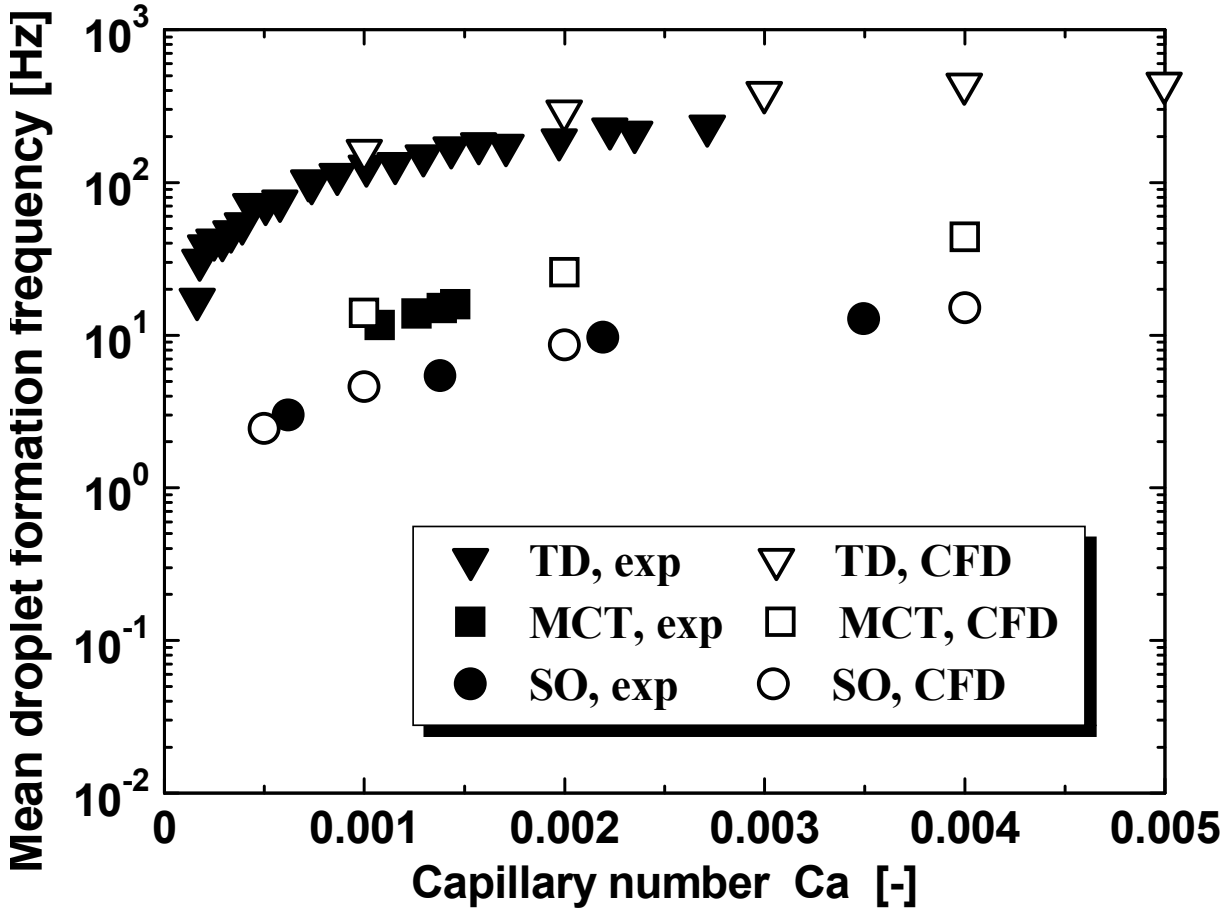


**Fig 11** Mean droplet generation rate from active channels vs. capillary number for tetradecane (TD), MCT oil (MCT) and soybean oil (SO) – experimental data and CFD simulation data.



Vladisavljević, G.T., Kobayashi, I. and Nakajima, M (2011) Microfluid Nanofluid 10: 1999–1209

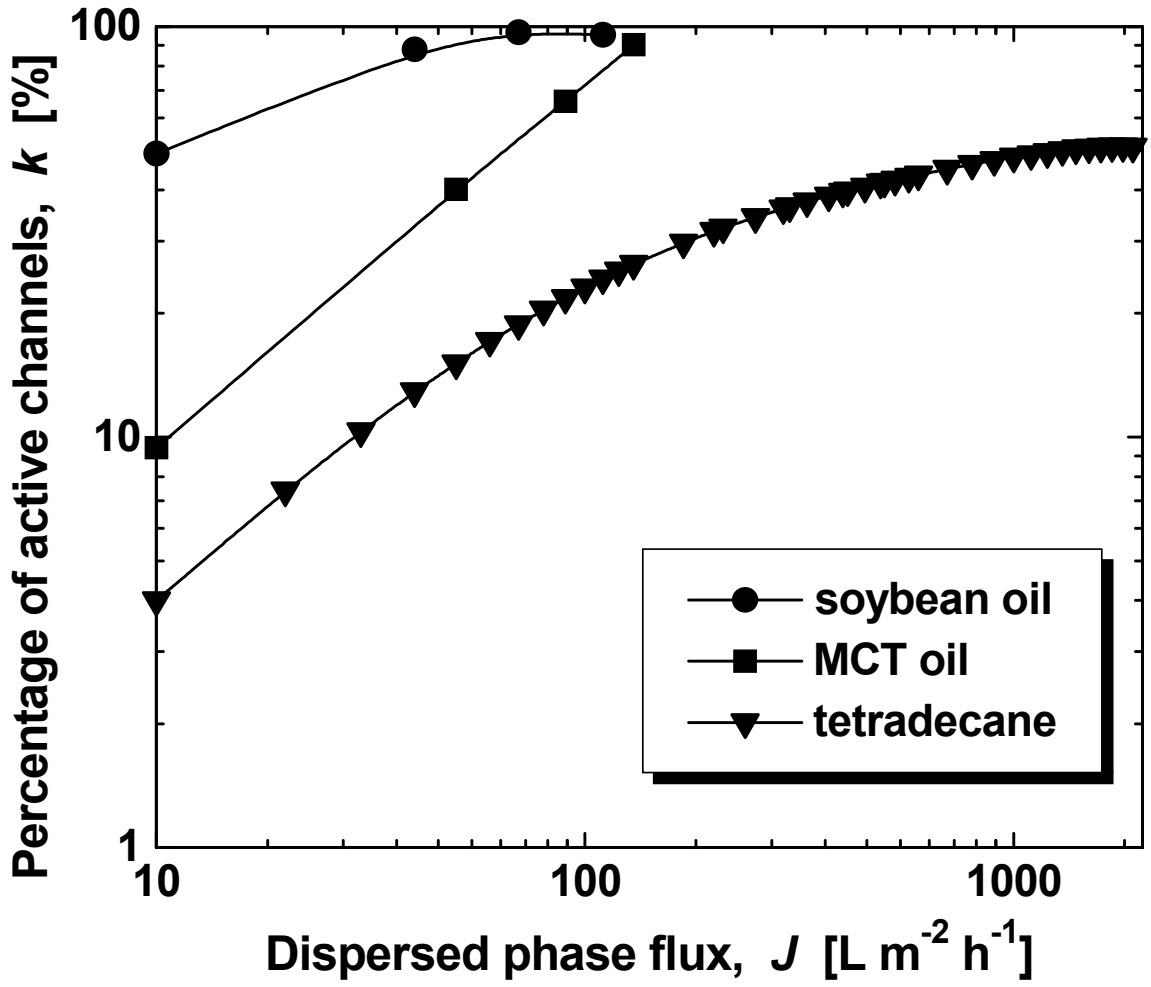


**Fig 12** Effect of dispersed phase flux on the percentage of active channels.



Vladisavljević, G.T., Kobayashi, I. and Nakajima, M (2011) Microfluid Nanofluid 10: 1999–1209

## Appendix

**Table A1** Typical transmembrane flux, mean droplet size and span of particle size distribution in membrane emulsification (ME). Dispersed phase: vegetable oil; continuous phase: 0.5–2% aqueous surfactant (Tween 20, Tween 80 or SDS) solution

| Method | Membrane | Droplet size and span | Flux | Authors |
|---|---|---|---|---|
| Repeated pre-mix ME | SPG, $d_p$ = 10.7 μm | $d_{50}$ =8.9–10.3 μm, span = 0.3–0.43 | 230,000–260,000 L $m^{-2}$ $h^{-1}$ at 1 vol% dispersed phase | Vladisavljević et al. (2006) |
| Cross-flow direct ME | SPG, $d_p$ = 1.4–6.6 μm | $d_{3,2}$=4.6–24 μm, span = 0.30–0.44 | < 80 L $m^{-2}$ $h^{-1}$ | Vladisavljević and Schubert (2003a) |
| Cross-flow direct ME | α-alumina, $d_p$ = 3.3–3.7 μm | $d_{3,2}$=4.6–24 μm, span = 0.42–0.56 | < 44 L $m^{-2}$ $h^{-1}$ | Vladisavljević and Schubert (2003b) |
| ME in stirred cell | Microsieve, $d_p$ = 20 μm, spacing=80–200 μm | $d_{50}$ =130-150 μm, span=0.19-0.8 | 2,000 L $m^{-2}$ $h^{-1}$ | Egidi et al. (2008) |

$$span = (d_{90} - d_{10}) / d_{50}$$



Vladisavljević, G.T., Kobayashi, I. and Nakajima, M (2011) Microfluid Nanofluid 10: 1999–1209

**Table A2** Typical plate dimensions, number of MCs, average size of resultant droplets and maximum throughput of grooved and straight-through silicon MC plates

| | **Grooved MC cross-flow** | **Grooved MC dead end** | **Straight-through** |
|---|---|---|---|
| Typical plate size | 8×22.5 mm<br>60×60 mm | 15×15 mm<br>24×24 mm<br>40×40 mm | 15×15 mm<br>24×24 mm<br>40×40 mm |
| Channel number | Up to 12,000 | 100–1,500 | 5,000–210,000 |
| Average droplet diameter | 1–100 μm | 1–100 μm | 4–50 μm |
| Maximum droplet generation frequency per module* | $<5\times10^5$ droplets $s^{-1}$ | $<8\times10^3$ droplets $s^{-1}$ | $<5\times10^5$ droplets $s^{-1}$ |
| Maximum dispersed phase flow rate* | 1.5 mL $h^{-1}$ | 0.1 mL $h^{-1}$ | 50 mL $h^{-1}$ |

*For triglyceride oil-in-water emulsion



Vladisavljević, G.T., Kobayashi, I. and Nakajima, M (2011) Microfluid Nanofluid 10: 1999–1209

**Table A3** The average droplet size, CV of droplet diameter and droplet throughput in straight-through MC emulsification (disperse phase: soybean oil; continuous phase: 1% SDS)

| MC plate | Channel number and size, b×a | Average droplet size and CV | Maximum droplet throughput | Authors |
|---|---|---|---|---|
| 24×24 mm, symmetric | 4,300 MCs, 9.6×48.7 μm | $d_{av}$=39.1 μm, CV=2.5% | 6 mL $h^{-1}$, $5.3\times10^{4}$ droplets $s^{-1}$ | Kobayashi et al. (2003) |
| 24×24 mm, symmetric | 10,000 MCs, 10.8×40.8 μm | $d_{av}$=41.9 μm, CV=1.9% | - | Kobayashi et al. (2004) |
| 40×40 mm, symmetric | 211,248 MCs, 6.6×26.7 μm | $d_{av}$=31–32 μm, CV<10% | 20–30 mL $h^{-1}$, $(3.2–5.3)\times10^{5}$ droplets $s^{-1}$, 3.3 droplets $s^{-1}$ per active MC | Kobayashi et al. (2005a) |
| 15×15 mm, symmetric | 23,548 MCs, 2.3×10.0 μm | $d_{av}$=6.7 μm, CV=3.9% | $5\times10^{-2}$ mL $h^{-1}$, $8.8\times10^{4}$ droplets $s^{-1}$, 3.8 droplets $s^{-1}$ per active MC | Kobayashi et al. (2008a) |
| 15×15 mm, symmetric | 92,575 MCs, 1.0×4.6 μm | $d_{av}$=4.4 μm, CV=5.5% | $4\times10^{-3}$ mL $h^{-1}$, $2.8\times10^{4}$ droplets $s^{-1}$, 30 droplets $s^{-1}$ per active MC | Kobayashi et al. (2008a) |
| 24×24 mm, asymmetric | 10,313 MCs, 11×104 μm | $d_{av}$=35 μm, CV=1.9% | 10 droplets $s^{-1}$ per active MC | Kobayashi et al. (2005b) |
| 24×24 mm, asymmetric stainless steel | 7 MCs, 300 μm × 13 mm | $d_{av}$=1.43 mm*, CV=4.4% | 0.11 droplets $s^{-1}$ per active MC | Kobayashi et al. (2008b) |

*Continuous phase: 1% bovine serum albumin (BSA)